scientific reports

Check for updates

OPEN

# Green-synthesized silver nanoparticle-enhanced nanofiltration mixed matrix membranes for high-performance water purification

Nusrat Bashir[1], Muhammad Afzaal[1]✉, Asim Laeeq Khan[2], Rab Nawaz[3,4], Ali Irfan[5]✉, Khalid S. Almaary[6], Fakhreldeen Dabiellil[7]✉, Mohammed Bourhia[8] & Zulkifl Ahmed[9]

**This study presents the fabrication and characterization of mixed matrix membranes (MMMs) incorporating green-synthesized silver nanoparticles (AgNPs) using *Hibiscus Rosa sinensis* extract within a polyethersulfone (PES) matrix for nanofiltration (NF) application. The membranes were evaluated for their pure water permeability, salt rejection, dye removal, and antifouling performance. Results showed that the membrane with 0.75 wt% AgNPs exhibited the highest pure water permeability of 36 L/m$^2$ h$^{-1}$ bar$^{-1}$ attributed to increased porosity and enhanced hydrophilicity. Addition of 0.75wt% AgNPs resulted in significant improvements, with NaCl rejection increased from 32 to 57%, $MgSO_4$ from 26 to 67%, and $CaCl_2$ from 27 to 41%. Antifouling tests revealed that the 0.75 wt% AgNPs membrane had the lowest irreversible fouling and highest flux recovery due to the antimicrobial action and improved surface properties of AgNPs. Importantly, the performance of the fabricated membranes align with loose nanofiltation characteristcs, as evidence by high dye rejection rates coupled with moderate rejection of salts. This study highlights the potential of green-synthesized AgNPs as effective nanofillers for developing high-performance and environmentally sustainable membranes into wastewater treatment.**

**Keywords** Nanofiltration, Green synthesis, Mixed matrix membranes, Silver nanoparticles, Wastewater treatment, Nanofiltration

The rapid growth in urbanization and population has worsened global water scarcity, making access to clean water a critical challenge[1]. Industrialization, coupled with the rise in urban waste, has resulted in significant contamination of water sources, further complicating efforts to secure safe and reliable water supplies[2]. Industrial effluents, often laden with complex and toxic pollutants such as heavy metals, persistent pollutants, dyes and salts, contribute heavily to the degradation of aquatic ecosystem's health and aesthetic quality[3]. Efficient and sustainable water treatment solutions are thus urgently needed to tackle these emerging challenges.

Several technologies have been developed to address wastewater treatment, including biological treatment, chemical coagulation, and adsorption[4,5]. While these methods offer varying degrees of effectiveness, they often suffer from limitations such as high energy consumption, chemical use, or the generation of secondary waste. In contrast, membrane technology, particularly nanofiltration, stands out as one of the most sustainable solutions[6]. Nanofiltration membranes are highly efficient in selectively removing contaminants while offering advantages

[1]Sustainable Development Study Centre, Government College University Lahore, Lahore 54000, Punjab, Pakistan. [2]Department of Chemical Engineering, Faculty of Engineering, Islamic University of Madinah, Madinah, Saudi Arabia. [3]Department of Environmental Sciences, The University of Lahore, Lahore 54000, Pakistan. [4]Faculty of Engineering and Quantity Surveying, INTI International University, Nilai 71800, Negeri Sembilan, Malaysia. [5]Department of Chemistry, Government College University Faisalabad, Faisalabad 38000, Pakistan. [6]Department of Botany and Microbiology, College of Science, King Saud University, P. O. BOX 2455, Riyadh 11451, Saudi Arabia. [7]University of Bahr el Ghazal, Freedowm Stree, Wau 91113, South Sudan. [8]Laboratory of Biotechnology and Natural Resources Valorization, Faculty of Sciences, Ibn Zohr University, Agadir 80060, Morocco. [9]College of Resource and Civil Engineering, Northeast University, Shenyang, China. ✉email: dr.afzaal@gcu.edu.pk; raialiirfan@gmail.com; researcherzem@gmail.com

such as low energy requirements, minimal chemical additives, high water recovery rates, and the ability to operate under moderate pressure conditions[7]. Loose nanofiltration (LNF) membranes effectively remove organic pollutants, dyes, and salts while maintaining high permeability. A newer development than traditional nanofiltration, LNF, offers high flux, moderate contaminant rejection, and reduced fouling, making it ideal for cost-effective industrial wastewater treatment[8].

Both polymeric and inorganic materials are commonly employed in membrane fabrication for wastewater treatment, each offering distinct merits and demerits. Inorganic materials, such as ceramic and metal oxide membranes, are known for their excellent thermal and chemical stability, but their high cost and brittle nature can limit widespread application[9]. Polymeric materials, on the other hand, are favored for their flexibility, ease of processing, and cost-effectiveness[10]. Among polymeric materials, polyethersulfone (PES) has emerged as a leading candidate due to its superior mechanical strength, chemical resilience, and thermal stability[11–13]. Despite these advantages, PES membranes face critical challenges that limit their performance. First, their hydrophobic nature makes them prone to fouling, which reduces water permeation rates and shortens membrane lifespan. Second, PES membranes exhibit poor stability, particularly under harsh operational conditions, which compromises their long-term durability. Fouling from the buildup of organic and inorganic substances is a major issue for polymeric membranes in wastewater treatment. To address this, approaches like surface modifications (grafting or coating) and blending PES with hydrophilic or nanomaterials have been studied[14]. These methods improve membrane hydrophilicity, decrease fouling, and enhance performance, leading to a longer lifespan and greater effectiveness in treating industrial wastewater.

Mixed matrix membranes (MMMs) represents a promising advancement in high-performance membranes, offering enhanced separation efficiency and resistance to fouling[15]. By incorporating inorganic or organic nanoparticles into a polymer matrix, MMMs combine the benefits of both materials, significantly improving permeability, selectivity, mechanical strength, and fouling resistance for more effective separation processes[16]. The phase inversion method is commonly used to fabricate LNF polymeric membranes due to its simplicity and versatility[17]. Commonly used nanomaterials in MMMs include metal-organic frameworks (MOFs), carbon nanotubes, silica nanoparticles, and metal oxides such as titanium dioxide ($TiO_2$) and zinc oxide (ZnO)[16,17]. However, many of these nanomaterials are synthetic and do not support green chemistry, which aims to reduce the environmental impacts. To achieve sustainability in membrane technologies, it is essential to incorporate nanomaterials that adhere to the principles of green chemistry and engineering. Sustainable alternatives, such as biogenic nanoparticles or those synthesized through eco-friendly methods, can enhance both the performance and sustainability of MMMs, contributing to more eco-friendly and effective water treatment solutions.

Green synthesis using plant extracts has gained considerable attention as an eco-friendly alternative for producing nanoparticles, offering simplicity, scalability, and reduced environmental impact compared to microbial or chemical methods[18–20]. Plant extracts contain a variety of bioactive compounds, such as proteins, flavonoids, phenolic acids, quercetin, and other polyphenolic substances, which act as natural reducing and capping agents. These compounds facilitate the reduction of metal salts into nanoparticles by stabilizing them and controlling their size and morphology during synthesis[21–25]. Among green-synthesized nanoparticles, silver nanoparticles (AgNPs) have been particularly promising due to their well-known antimicrobial properties and their ability to enhance membrane performance through improved antifouling resistance and promote effective pollutant rejection, making them ideal for water treatment applications[26]. In a study conducted by Alnairat et al.[27] the green synthesized AgNPs were incorporated into PVDF ultrafiltration membranes which showed excellent antibiofouling behavior and Bovine serum albumin (BSA) rejection. In another study, AgNPs were synthesized from P. speciosa peels and seeds and mixed with polysulfone[28]. The best results were obtained with 0.1 wt% filler, showing a crystallite size of 51.60 nm, finger-like hollow spaces averaging 15.23 µm in diameter, a mean pore size of 10.20 nm. This combination resulted in a contact angle of 63.30°, indicating hydrophilicity, a permeation flux of 327.73 L $m^{-2}$ $h^{-1}$, a rejection rate of 67.21%, and minimal leaching of AgNPs after filtration. In an another study, AgNPs using Verbascum thapsus leaf (VTL) were impregnated on a UP150 membrane which showed excellent antioxidant activities (87% DPPH) and 100% metal chelating activities along with strong antimicrobial activities against *E. coli* and 81.29% biofilm inhibition against *S. aureus* and *P. aeruginosa*[29]. PES membrane coated with Ag NPs was also tested for its antimicrobial efficacy and *E. coli* removal. However, there remains considerable research gap regarding the optimizing of green synthesis process to achieve better control over nanoparticle size, distribution, and overall performance. Further studies are required to fully understand their long-term stability in membranes and their effectiveness in enhancing pollutant rejection and antifouling characteristics in real-world conditions.

This study focuses on the fabrication of MMMs that incorporate green-synthesized AgNPs derived from the floral extract of *Hibiscus Rosa sinensis* into a PES matrix. This novel approach merges sustainable nanoparticle synthesis with advanced membrane technology, addressing key in wastewater treatment. By utilizing AgNPs produced through an eco-friendly method, the research aims to create high-performance membranes with improved antifouling properties, pollutant rejection, and durability. The choice of *Hibiscus Rosa sinensis* as a natural reducing and stabilizing agent not only promotes green chemistry but also offers a scalable, cost-effective method for nanoparticle synthesis. The novelty of this approach lies in its integration of green chemistry principles into membrane technology, making this study a critical contribution toward the creation of more robust, eco-friendly solutions for water purification.

## Materials and methods

### Materials

All chemicals used in this study were of analytical grade. Silver nitrate ($AgNO_3$, Mw 169.9 g/mol) and N-Methyl-2-pyrrolidone (NMP, Mw 99.13 g/mol) as the solvent were sourced from Sigma-Aldrich. The polymer, PES (Ultrason E 6020P, Mw 72,000 g/mol), was purchased from BASF Co., Germany. Additional chemicals used

include sodium chloride (NaCl, Mw 58.44 g/mol), calcium chloride ($CaCl_2$, Mw 110.98 g/mol), and magnesium sulfate ($MgSO_4$, Mw 138.38 g/mol) were also purchased from Sigma- Aldrich. A non-woven polypropylene/polyethylene (PP/PE) fabric sheet (Novatexx-2471) was kindly provided by Freudenberg, Germany, and used as support material for membrane casting. Fresh flowers of *Hibiscus Rosa sinensis* were collected from the tropical regions of Lahore, Pakistan, and used for the green synthesis of silver nanoparticles. Deionized water (DI) with a resistivity of 18.2 MΩ cm was obtained using a purification system and used for all experimental procedures.

## Preparation of green synthesized silver nanoparticles

The green synthesis of silver nanoparticles (AgNPs) from metallic salts is a simple, eco-friendly process that involves natural oxidation-reduction reactions. In this study, AgNPs were synthesized using *Hibiscus Rosa sinensis* flower extract, following a modified procedure based on previous studies[30] with optimizations to improve yield and quality. Freshly cut *Hibiscus Rosa sinensis* flowers (20 g) were boiled in 100 mL of deionized water at 80 °C for 2 h to obtain the plant extract. After cooling, the extract was filtered through Whatman grade 1 filter paper and stored at 4 °C for future use. To initiate the green synthesis, 20 mL of the flower extract was added to 90 mL of 1 mM $AgNO_3$ solution, and the pH of the mixture was adjusted to 6. Upon mixing, the solution gradually turned dark brown, indicating the formation of silver nanoparticles. The solution was then incubated for 24 h and centrifuged at 12,000 rpm for 15 min. The resulting nanoparticles were washed three times with ethanol or deionized water to remove impurities. The purified nanoparticles were freeze-dried and subsequently ground into a fine powder using a pestle and mortar for further use. Figure 1 provides a schematic representation of the green synthesis process of silver nanoparticles using *Hibiscus Rosa sinensis* extract.

## Fabrication of mixed matrix membranes

The green-synthesized AgNPs were embedded as fillers in the fabrication of MMMs. The phase inversion technique was employed for membrane fabrication due to its ease of morphology control, scalability and widespread use in industrial applications. To prepare pristine membranes, a casting solution was created by dissolving 22 wt% PES in a solvent mixture consisting of 78 wt% N-Methyl-2-pyrrolidone (NMP) and Tetrahydrofuran (THF) in a 3:1 ratio. In the case of MMMs, varying concentrations of the AgNPs (0.25 wt%, 0.5 wt%, 0.75 wt%, and 1 wt%) were dispersed in NMP and stirred for 2 h to ensure thorough distribution of the nanoparticles. Afterwards, the required amount of polymer in THF was added to the mixture in parts. To prevent nanoparticle aggregation, the polymer was added in the suspension containing AgNPs in several parts (10%, 20%, 20%, and 50% of the total required quantity) following priming protocol. This stepwise approach ensured better dispersion of the nanoparticles, minimizing the risk of clumping and promoting a more uniform distribution within the polymer

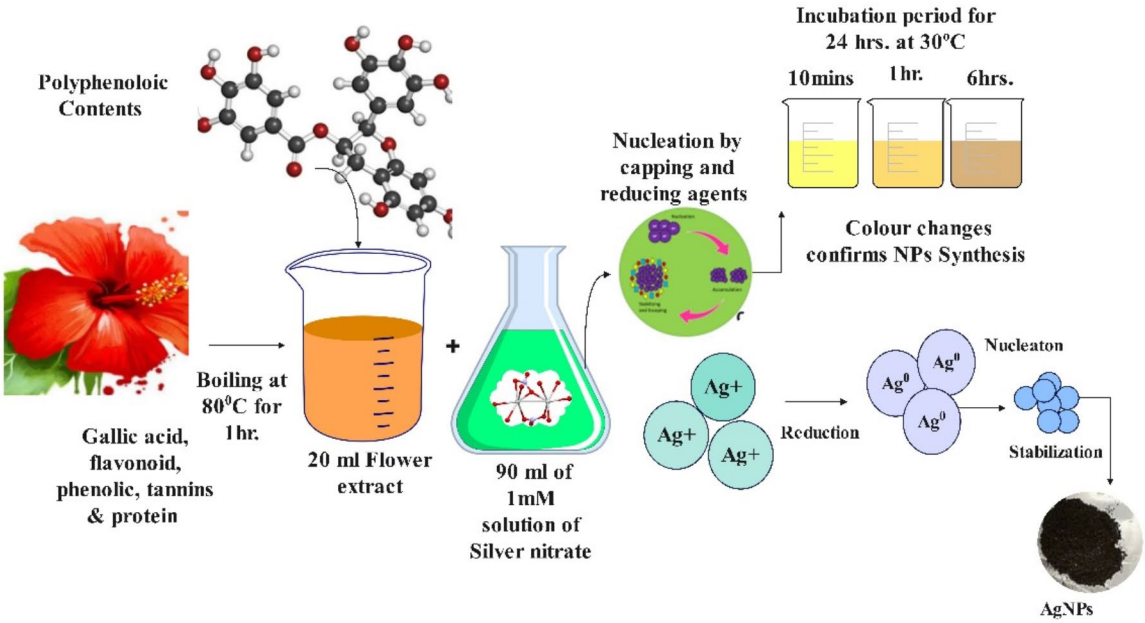


**Fig. 1**. Representation of green synthesis of AgNPs.

matrix. Following this, the dope solution was stirred continuously at ambient temperature for 24 h at room temperature to achieve a homogeneous solution with further stabilization of dispersion. Although the visible dissolution of polymer was observed within couple of hours, the solution was left to stir for an entire day to ensure complete dissolution of large polymer chains. The solution was left overnight to release any trapped air bubbles.

A non-woven polypropylene/polyethylene (PP/PE) fabric sheet (Novatexx-2471) was affixed to a glass plate to provide smooth and rigid surface. The non-woven substrate is necessary to provide mechanical stability and operation at high pressures in the range of NF applications. NMP was spread over it to prevent the polymer solution from penetrating the pores of the fabric. Membranes were cast using an automatic film applicator (Elcometer, UK) with a metallic applicator, ranging film casting thickness of 250 µm. After 30 s of evaporation, which allowed the active layer to densify, the glass plate was immersed in a coagulation bath filled with distilled water for 15 min to complete the phase inversion process and solidification of the membrane film. The fabricated membranes were subsequently labeled and stored in containers filled with deionized water to remove any residual solvents. The membranes were stored in water for 48 h to stabilize their structure and ensure complete removal of solvent before performance assessment.

The composition details of the prepared membranes are provided in Table 1.

## Characterizations techniques

Fourier Transform Infrared (FT-IR) spectroscopy was employed to identify the functional groups and chemical interactions in both the synthesized AgNPs and the MMMs. A Thermo-Nicolet 6700 P FT-IR spectrometer (USA), equipped with helium gas purging, was used for the analysis. Measurements were conducted in absorbance mode, with a resolution range of 0–100 nm, over 256 scans, and a spectral range from 400 to 4000 $cm^{-1}$. To examine the crystallinity of the AgNPs and MMMs, X-ray Diffraction (XRD) analysis was performed using a PANalytical X'Pert Pro PW3050/60 diffractometer manufactured by Philips (Malvern, UK). The instrument was operated at 45 kV and 40 mA, using CuKα radiation ($\lambda = 0.1540$ nm). The analysis covered a scanning range (2θ) from 5° to 80°, with a step size of 0.02° and a scan time per step of 0.65 s, for a total counting time of 1200 s. The hydrophilicity of the fabricated membranes was assessed through Water Contact Angle (WCA) measurements, using Biolin Scientific Attention Theta Flex Analyzer contact angle meter. A 2 µL droplet of deionized water was placed on the surface of each membrane, and the static contact angle was recorded immediately. The measurements were conducted at room temperature (25 °C ± 5 °C), and readings were taken at three different points on each membrane to obtain an average value, providing a quantitative measure of the surface wettability and hydrophilic properties of the membranes. Morphological details of the MMMs were analyzed using SEM utilizing a Field Emission Scanning Electron Microscope (FEI Nova 450 NanoSEM). For comprehensive cross-sectional analysis, membrane samples were peeled off from non-woven fabric and then a small piece of membrane was cryogenically cut into the liquid nitrogen. The fractured sample was then placed on a sample stub using carbon tape. To enhance conductivity and prevent charging during scanning, all samples were subsequently coated with a thin layer of gold. This sample preparation technique is crucial for obtaining high-quality SEM images. The study of the surface charges on the prepared MMMs were analyzed by Zeta potential using Zeta Sizer, version 7.12 (Malvern, UK).

## Membrane performance

The pure water permeability (PWP) of both the pristine and modified membranes was evaluated using a dead-end filtration setup (HP4750 Stirred Cell, STERLITECH Corporation, USA). In each test, approximately 200 mL of deionized water was placed into the filtration cell, which was connected to a nitrogen gas cylinder to apply pressure. The working pressure was maintained at 9 bar throughout the experiment. The filtration cell was placed on a magnetic stirrer to ensure uniform mixing of the water feed. Before measuring the PWP, the membranes underwent a 30-minute compaction period to achieve stable flow conditions. Once steady flux was reached, the PWF was calculated using the following formula:

$$Jo = (V/(A \times \Delta t \times p)) \quad (1)$$

where $J_0$ is the PWF ($Lm^{-2}h^{-1}$ $bar^{-1}$), V is volume of permeate (L), A denotes effective area of membrane ($m^2$) and Δt is permeation time (h).

To evaluate the salt rejection performance of the membranes, separate feed solutions of sodium chloride (NaCl), magnesium sulfate ($MgSO_4$), and calcium chloride ($CaCl_2$) were prepared at a concentration of 1000 ppm. The

| Membranes | PES wt% | NMP wt% | THF wt% | AgNPs wt% |
|---|---|---|---|---|
| M-0 (neat) | 22.0 | 58.5 | 19.5 | 0 |
| M-1 | 22.0 | 58.5 | 19.5 | 0.25 |
| M-2 | 22.0 | 58.5 | 19.5 | 0.50 |
| M-3 | 22.0 | 58.5 | 19.5 | 0.75 |
| M-4 | 22.0 | 58.5 | 19.5 | 1 |

**Table 1**. Formulation details of the prepared membranes.

pH of the salt's feed solution was noted using pH meter (Hanna Instruments, USA), which was in between 6 and 6.5 for all salts. Salts are generally neutral compounds that do not significantly alter the pH of their solutions when dissolved in water. Upon dissolution, these salts dissociate without undergoing hydrolysis, resulting in solutions that maintain a near-neutral pH range of 6–6.5, as observed in our study. The conductivity of the permeate was measured using a conductivity meter (Hanna Instruments, USA).

The rejection of salts was calculated using the following equation:

$$R\,(\%) = (1 - \frac{Cp}{Cf}) \times\ 100 \tag{2}$$

where R is the salt rejection percentage (%), $C_p$ is the concentration of the salt in the permeate, and $C_f$ is the concentration of the salt in the feed solution.

The rejection performance of the membranes for dyes was evaluated using methylene blue (Mw = 319.85 g/mol), Congo red (Mw = 696.66 g/mol), and Rose Bengal (Mw = 973.67 g/mol) as model pollutants. Feed solutions of each dye were prepared at an initial concentration of 30 ppm. The UV absorbance of the permeate was measured using a UV-spectrophotometer (BMS-UV-1602) to determine the concentration of the dye in the permeate. The rejection was calculated using the Eq. (2) with $C_p$ and $C_f$ representing the concentration of respective dye in permeate and feed respectively.

The antifouling performance of the membranes was evaluated using a 1000 ppm Sodium Algenate solution as the foulant. Initially, the PWF was measured to establish a baseline. Afterward, the sodium alginate solution was passed through the membrane under the same conditions to simulate fouling. The membrane was then removed and rinsed with deionized water for 30 min to remove any loosely bound foulants. Following the cleaning process, the PWF was measured again to assess the membrane's recovery. The flux recovery ratio (FRR) is used to quantify the membrane's ability to recover its flux after cleaning, expressed as a percentage of the initial pure water flux before fouling ($J_w$). The reversible fouling ratio ($R_r$) represents the portion of fouling that can be removed by cleaning, calculated by comparing the flux after cleaning ($J_c$) with the flux after fouling ($J_p$) and the initial pure water flux ($J_w$). The irreversible fouling ratio ($R_{ir}$) measures the fraction of fouling that remains even after cleaning, indicating permanent damage to the membrane. The total fouling ratio ($R_t$) provides an overall measure of the fouling experienced by the membrane.

The fouling resistance was quantified using the following formulas:

$$FRR\ (\%) = (JC/Jw) \times\ 100 \tag{3}$$

$$Rr\,(\%) = (JP/Jw) \times\ 100 \tag{4}$$

$$Rir\ (\%) = (Jw - \frac{Jc}{Jw}) \times\ 100 \tag{5}$$

$$Rt = (Jw - Jp/Jw \tag{6}$$

## Results and discussion

### Characterization of green synthesized nanoparticles

FT-IR spectroscopy was employed to identify the functional groups responsible for the synthesis and stabilization of the green-synthesized AgNPs. This technique plays a crucial role in revealing the biomolecules involved in reducing metal ions and stabilizing the nanoparticles during green synthesis. In the present work, the FT-IR spectrum of *Hibiscus rosa-sinensis crude flower* extract reveal key peaks at 3357 $cm^{-1}$, 2175 $cm^{-1}$, and 1639 $cm^{-1}$ correspond to hydroxyl, carbonyl, and carboxylic groups, respectively, which are crucial in reducing and capping the silver nanoparticles (Fig. 2a). The FT-IR spectrum of the synthesized AgNPs exhibited distinct peaks corresponding to functional groups involved in their formation. A prominent peak at 3258 $cm^{-1}$ corresponds to O-H stretching vibrations, indicating the presence of polyphenolic compounds. These polyphenols, known for their antioxidant properties, play a key role in reducing metal ions to form nanoparticles while simultaneously acting as stabilizing agents to prevent agglomeration, ensuring long-term stability of the synthesized AgNPs. Additional important peaks were observed at 2920 $cm^{-1}$, 1580 $cm^{-1}$, 1296 $cm^{-1}$, 1024 $cm^{-1}$, and 688 $cm^{-1}$. The peak at 2920 $cm^{-1}$ is attributed to C-H stretching vibrations, commonly associated with aliphatic hydrocarbons. The peak at 1580 $cm^{-1}$ corresponds to C = C stretching vibrations, likely linked to the aromatic nature of the polyphenolic structures present in the plant extract. The peaks at 1296 $cm^{-1}$ and 1024 $cm^{-1}$ indicate C-O stretching and bending vibrations, further confirming the presence of oxygen-containing functional groups. These functional groups are essential for the synthesis and stabilization of AgNPs, as they are involved in the reduction of metal ions and act as capping agents to prevent nanoparticle aggregation[31,32]. Carbonyl compounds and proteins are essential in the synthesis and stabilization of AgNPs. The amine groups in proteins play a key role in nanoparticle formation and functionalization, acting as reducing agents and stabilizers to facilitate synthesis and prevent aggregation[33]. Polyphenols play a key role in preserving the nanostructures and highlights the essential biomolecules in the green synthesis of AgNPs[34,35]. This comprehensive analysis reinforces the importance of polyphenols, proteins, and other biomolecules in facilitating the green synthesis and stabilization of AgNPs.

The crystalline structure and degree of crystallinity of the green-synthesized AgNPs were determined using XRD analysis. XRD is a highly effective method for both qualitative and quantitative assessment of nanoparticles, providing crucial information about the formation of crystalline structures and the purity of the synthesized

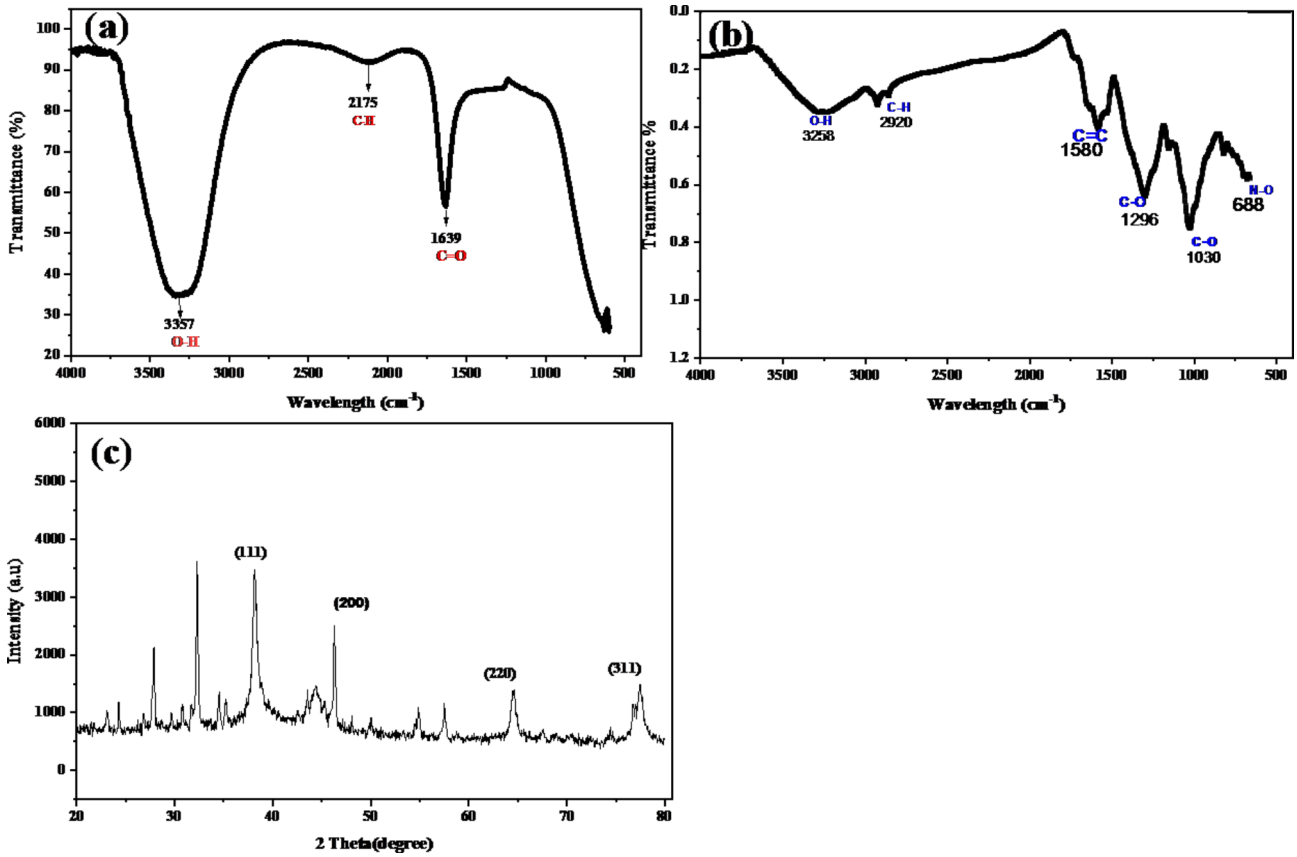


**Fig. 2**. Characterizations of green synthesized Silver Nanoparticles (AgNPs), (**a**) FTIR for flower extract (**b**) FTIR for Silver nanoparticles (**c**) XRD of green synthesized AgNPs.

nanoparticles, while also identifying the presence of impurities[38]. Figure 2c presents the XRD pattern of the synthesized AgNPs, where distinct diffraction peaks were observed at 2θ values of 38.1°, 46.3°, 64.5°, and 77.4°, corresponding to the (111), (200), (220), and (311) planes, respectively[36,37]. These sharp and well-defined peaks are characteristic of the face-centered cubic (FCC) structure of silver, as previously reported in earlier studies[38,39]. Two additional diffraction peaks were observed at 32.1° and 27.8° (2θ), which could be attributed to organic compounds present in the plant extract used during the synthesis process. These organic compounds likely played a role in stabilizing the nanoparticles and facilitating the reduction of $AgNO_3$ to AgNPs. Similar findings were reported by earlier studies[40,41], suggesting that these additional peaks may originate from the biomolecules within the plant extract, which contribute to the formation and stabilization of the nanoparticles. The appearance of these additional peaks has also been documented in other studies involving the green synthesis of silver nanoparticles using various plant extracts, such as *Ctenolepis garcini L.*, *Eruca sativa*, *Spinacia oleracea*, *Brillantaisia patula*, *Crossopteryx febrifuga*, and *Senna siamea*[42,43]. These findings further support the use of plant-based organic compounds as reducing and stabilizing agents in the synthesis of AgNPs, which has been consistently demonstrated across numerous studies.

The surface morphology of the synthesized AgNPs was characterized using Scanning Electron Microscopy (SEM), while their elemental composition was analyzed through Energy Dispersive X-ray Spectroscopy (EDX). SEM images (Fig. 3a–c) revealed nanoparticles of varying sizes with some degree of aggregation, which can reduce the effective surface area, thereby impacting membrane performance. Proper dispersion of nanofillers is crucial, and spherical nanoparticles, especially those smaller than 100 nm, help minimize aggregation, leading to better distribution in the casting solution[44]. The average nanoparticle size was determined to be approximately 70 nm, which is ideal for maintaining uniformity within the polymer matrix. Agglomeration, although common in green synthesis, can reduce the surface area and affect the reactivity of the nanoparticles, as similarly reported by[45].

The EDX analysis confirmed the presence of silver as the primary component, along with chlorine, likely from the silver precursor or as a stabilizing agent (Fig. 2d). The spectrum supported the successful reduction of silver ions, consistent with observations made in other studies[46,47]. The size distribution of the nanoparticles, with a mean size of 70 nm (Fig. 3d), is in agreement with previous studies on silver nanoparticles synthesized from plant extracts[42].

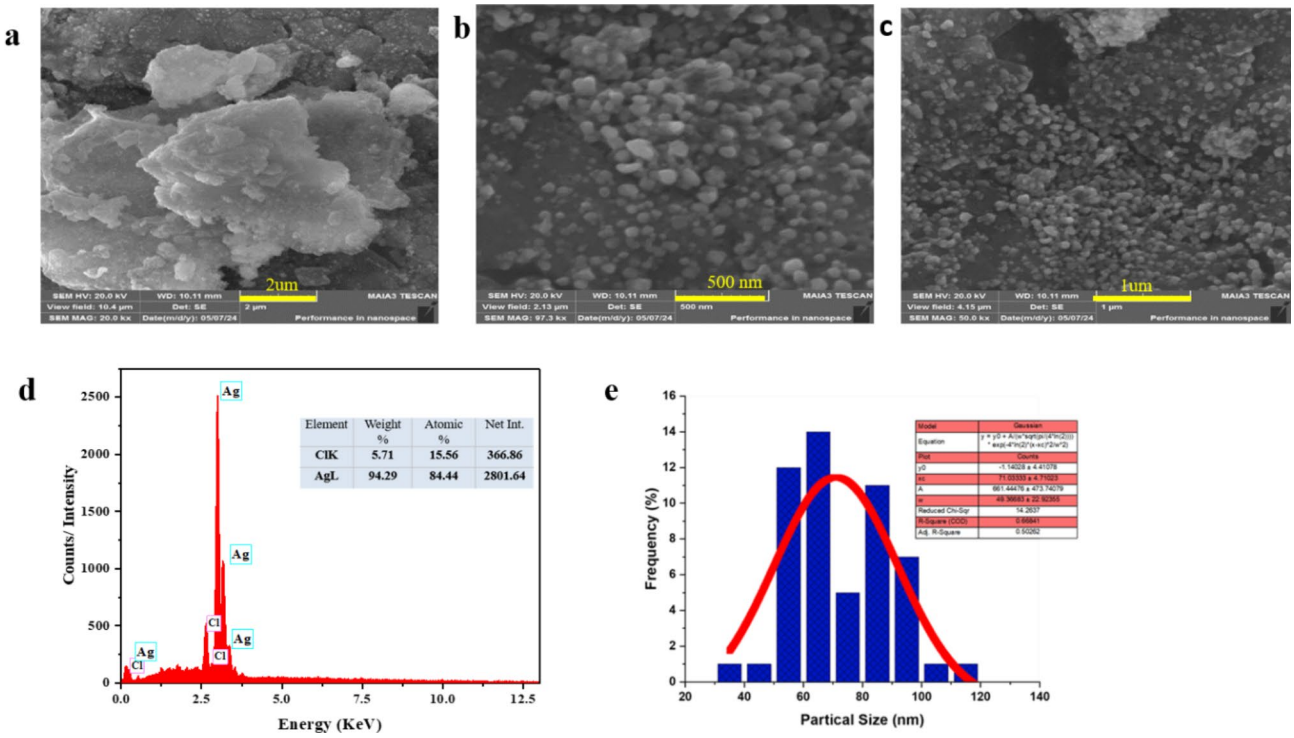


**Fig. 3**. SEM images of Green synthesized AgNPs at different magnifications (**a**–**c**), EDX analysis of AgNPs (**d**), Particle size distribution of AgNPs from SEM images (**e**).

## Characterization of fabricated membranes

FT-IR analysis was performed to identify the functional groups in both the pristine PES and MMMs. The O-H stretching band at 3372 $cm^{-1}$, present in both the pristine membrane and modified membranes, indicates the presence of hydroxyl groups, likely from water molecules, alcohols, and/or phenolic compounds. In M3, the slightly increased intensity of this peak suggests that the higher addition of green-synthesized silver nanoparticles enhances the membrane's hydrophilic properties. This increase in intensity may reflect a greater interaction of the membrane with water, potentially improving its hydrophilicity and filtration performance. In the pristine PES membranes, a distinct peak at 1638 $cm^{-1}$ corresponds to the stretching of aromatic rings in PES. After the incorporation of AgNPs, the intensity of this peak decreased, likely due to molecular interactions between the polymer matrix and the nanoparticles, suggesting the successful integration of AgNPs within the membrane. A peak at 1573 $cm^{-1}$, associated with N-O stretching from nitro compounds ($NO_2$), due to the presence of silver nanoparticles was observed[48], while a peak at 1480 $cm^{-1}$ was attributed to C-H bending vibrations from alkane groups or from aromatic rings of PES structure. These functional groups further confirm the successful modification of the PES membrane with AgNPs, enhancing its hydrophilicity and surface interactions, leading to improved membrane functionality.

The contact angle measurement is widely regarded as one of the most reliable methods for assessing the wettability of solid surfaces. Evaluating the hydrophilic or hydrophobic properties of membranes through water contact angle (WCA) measurements is crucial for predicting their overall performance, particularly in water purification processes. The pristine PES membrane used in this study exhibited a WCA of 76°, indicating moderate hydrophilicity, as shown in Fig. 4b. The incorporation of green-synthesized AgNPs into the PES matrix significantly improved the hydrophilicity of the membranes. As the concentration of AgNPs increased from 0.25 to 0.5 wt%, the WCA decreased from 66° to 63°, reflecting enhanced wettability. Further increasing the AgNPs content to 0.75 wt% and 1 wt% reduced the WCA to 61° and 59°, respectively. This trend clearly demonstrates a consistent increase in hydrophilicity with higher nanoparticle incorporation.

These findings align with previous studies[49], which reported enhanced membrane performance upon the incorporation of nanoparticles. The higher hydrophilicity observed in both virgin and modified membranes suggest that the latter could offer greater water permeability and reduced fouling, making them highly suitable for water filtration applications. The increase in hydrophilic character can be attributed to the incorporation of O-H stretching bands, as observed in the FTIR spectra. These bands, originating from the phenolic compounds in the green-synthesized AgNPs, suggest a higher density of hydroxyl groups on the nanoparticle surface. Since AgNPs synthesized through green methods inherently possess hydrophilic properties due to the plant extracts used (which are rich in hydroxyl groups), this combination effectively reduces the interfacial energy of the membrane, resulting in lower WCA values and enhanced hydrophilicity.

The surface charge of the fabricated membranes was evaluated using zeta potential measurements across multiple pH levels (3, 5, 7, and 9) with a 1 mM KCl electrolyte solution. As illustrated in Fig. 4c, the pristine PES

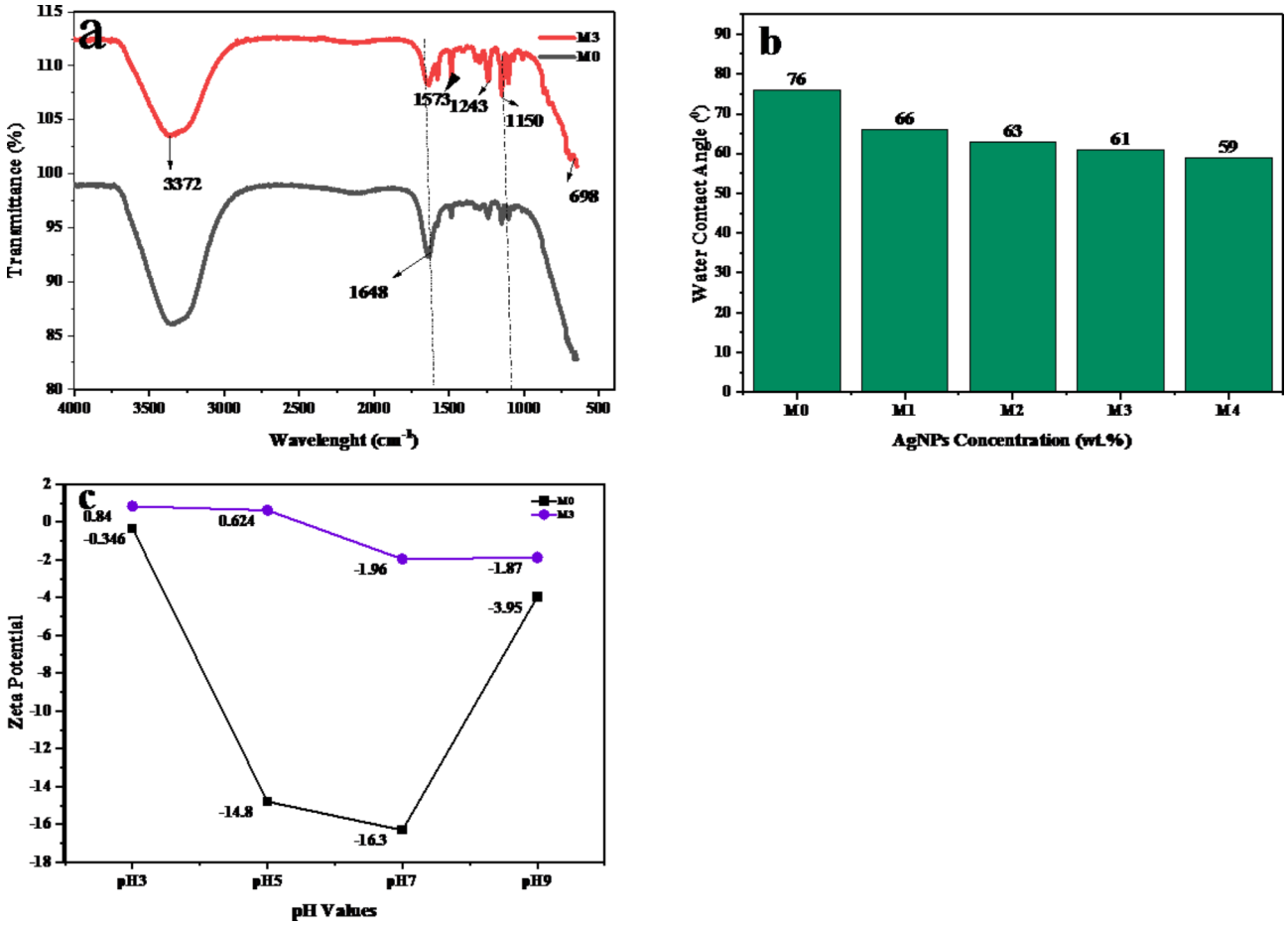


**Fig. 4**. Characterizations of fabricated PES/AgNPs, (**a**) FTIR of MMMs, (**b**) water contact angle of PES/AgNPs membranes, (**c**) zeta potential of neat membrane and 0.75wt% PES/AgNPs membrane.

membranes exhibited strongly negative charges as reported in earlier studies[50,51]. Upon the addition of AgNPs, the surface charge shifted toward more positive values at lower pH levels and became less negatively charged at neutral pH. This shift in surface charge can be attributed to the pH-dependent protonation effects and the introduction of AgNPs, which carry inherent positive charges ($Ag^+$). Additionally, the presence of amine groups, phenolic compounds, and proteins in the *Hibiscus Rosa sinensis* extract, which also contain positive charges, further influenced the zeta potential of the modified membranes. When AgNPs are added to the membrane matrix, they may form bonds or interact with these negatively charged sites, either through electrostatic attraction or by inducing local charge redistribution. These changes in zeta potential highlight the role of AgNPs in modifying the structural and surface properties of the membranes, enhancing their overall performance for filtration applications.

The SEM analysis of the membranes revealed their typical asymmetric structure, featuring a dense top layer and a more porous substructure, as shown in Fig. 5. In the pristine PES membrane, the top layer appeared dense with narrow, oblique, and short finger-like pores, that may lead to lower flux during filtration. This structure resulted from controlled evaporation and instantaneous demixing, leading to a tightly packed, pollutant-rejecting top layer. The addition of nanofillers led to a reduction in the top layer's thickness, while simultaneously creating a more porous membrane structure. AgNPs acted as porogen, introducing defects into the polymer chains and forming a more permeable membrane. As the concentration of AgNPs increased, the membrane porosity also increased, likely due to the formation of additional channels in the membrane structure. The SEM images clearly demonstrate an increased number and size of pores in the modified membranes, facilitating improved water permeability and higher permeability compared to the neat PES membranes. The enhanced hydrophilicity of AgNPs accelerated the solvent exchange during coagulation, promoting the formation of elongated, interconnected finger-like pores. This structural modification not only enhanced water permeability but also improved pollutant rejection. At an optimal concentration of 0.75 wt% AgNPs, the SEM images showed a more distinct finger-like pore structure, which corresponds with the observed increase in membrane hydrophilicity (as seen in the contact angle measurements). In contrast, higher than 0.75% concentrations of AgNPs led to particle aggregation and reduced effectiveness due to the formation of a denser, less porous structure. A very similar behavior was also reported in earlier studies[52].

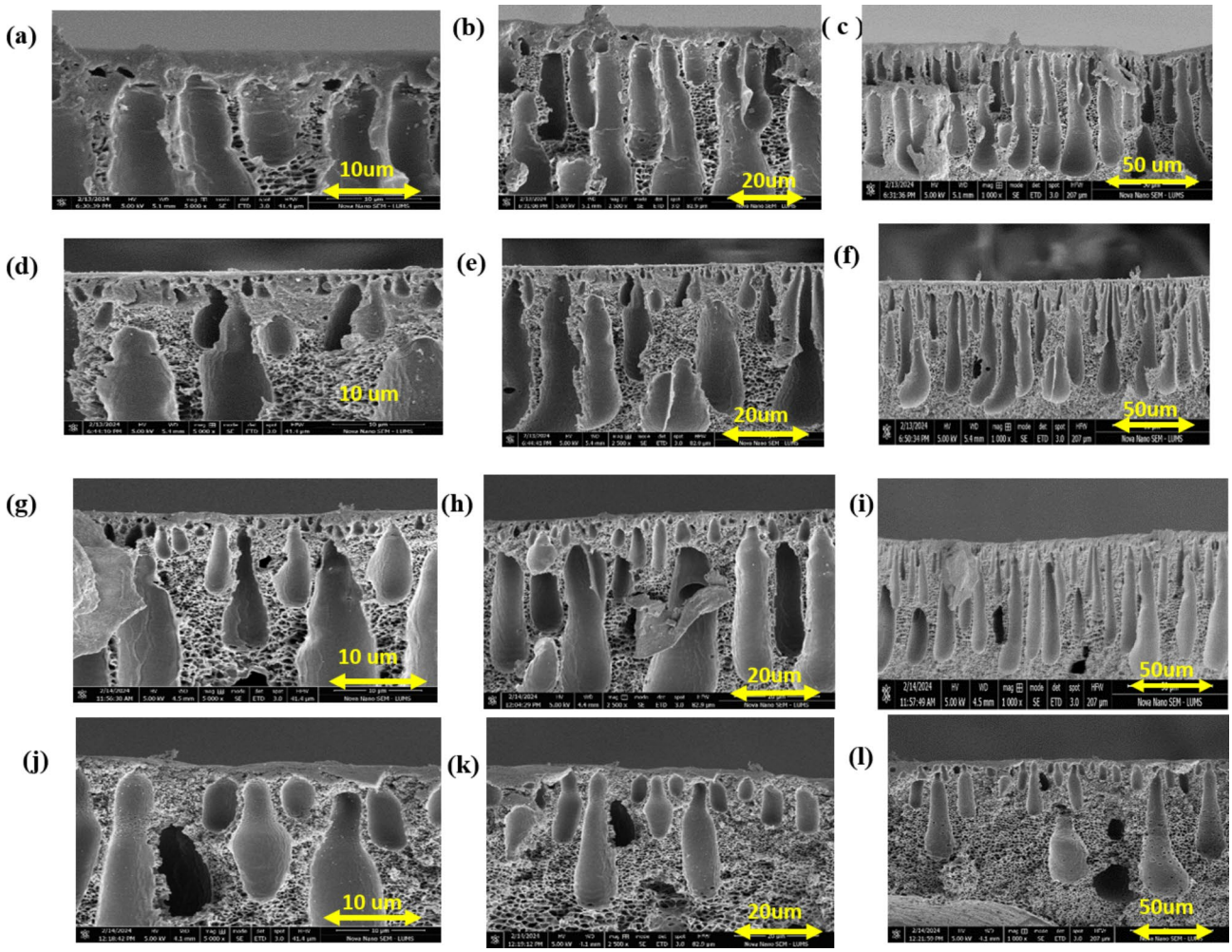


**Fig. 5**. Cross sectional SEM images of Neat membranes (**a**–**c**) 0.25wt% (**d**–**f**) 0.75wt% (**g**–**i**) and 1wt% PES/Ag NPs (**j**–**l**).

Upon increasing the concentration of AgNPs higher than 1 wt%, a decrease in water channels was observed. This reduction may be attributed to the aggregation of AgNPs within the membrane, which results in saturation and increased viscosity of the polymer solution. This reduction in permeability upon excessive incorporation of AgNPs beyond 1wt% is may be associated with limiting mass percentage. Beyond this threshold level, the nanoparticle begins to aggregate rather than uniformly dispersed in polymer matrix. This aggregation, particularly in the top layer, can create non-selective pathways, potentially compromising the filtration efficiency of the membranes. Moreover, at higher concentrations of 1 wt% AgNPs, the increased viscosity of the casting solution effects phase separation process which led to changes in the sublayer structure, with the appearance of more prominent sponge-like pores. This aggregation of nanoparticles generally causes pore blocking and the formation of non-uniform pore and denser structures, which hinders water permeability[52].

These results highlight the importance of balancing the concentration of AgNPs to enhance hydrophilicity and pore structure while maintaining optimal nanoparticle distribution within the polymer matrix. By doing so, the membranes can achieve superior filtration performance without compromising structural integrity or selectivity. Membranes loaded with AgNPs exhibited a clear asymmetric morphology, consisting of three distinct layers: a selective top layer, finger-like projections for permeation, and a bottom layer that provides mechanical strength (Fig. 6).

## Performance assessment of MMMs

Pure water permeability (PWP) is a crucial parameter for assessing membrane performance. The PWF of both neat and PES/AgNPs MMMs was evaluated using dead-end filtration at a pressure of 9 bar, after a 60-minute compaction period. As shown in Fig. 7a, the PWP of all MMMs was higher than that of the neat PES membrane. The membrane with 0.75 wt% AgNPs showed the highest PWP, increasing from 11 $L/m^2\,h^{-1}\,bar^{-1}$ in neat PES to 36 $L/m^2\,h^{-1}\,bar^{-1}$. This improvement can be attributed to several factors: enhanced porosity, increased antifouling capacity improved hydrophilicity, and reduced surface roughness due to the incorporation of hydrophilic AgNPs. The higher water uptake capacity of the green-synthesized AgNPs facilitated more water permeation, while the SEM analysis confirmed the formation of larger macro-voids in the membrane structure, reducing

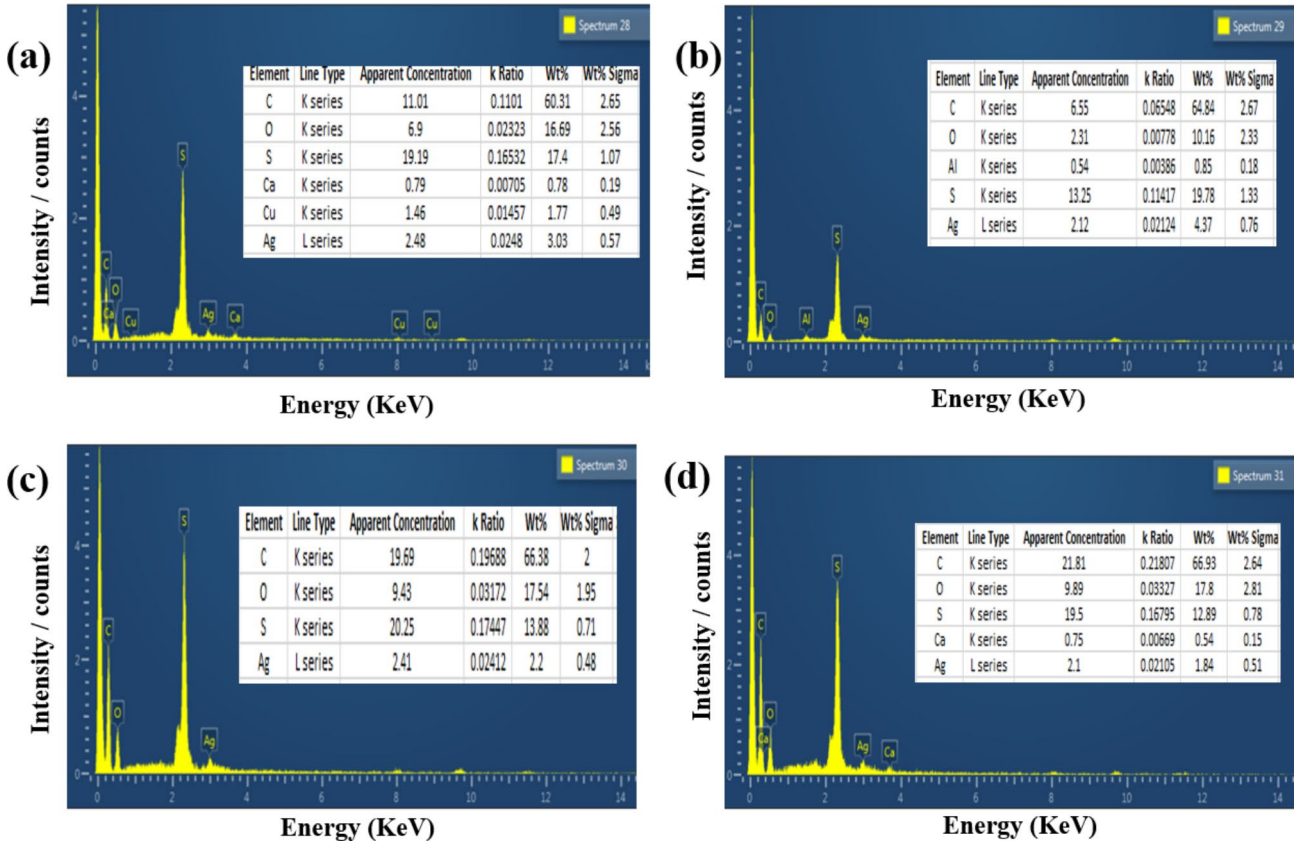


**Fig. 6**. Energy–dispersive X-ray spectroscopy EDX of fabricated MMMs, (**a**) 0.25wt% (M1) PES/AgNPs. (**b**) 0.5wt% (M2) PES/AgNPs. (**c**) 0.75wt% (M3) PES/AgNPs. (**d**) 1wt% (M4) PES/AgNPs/.

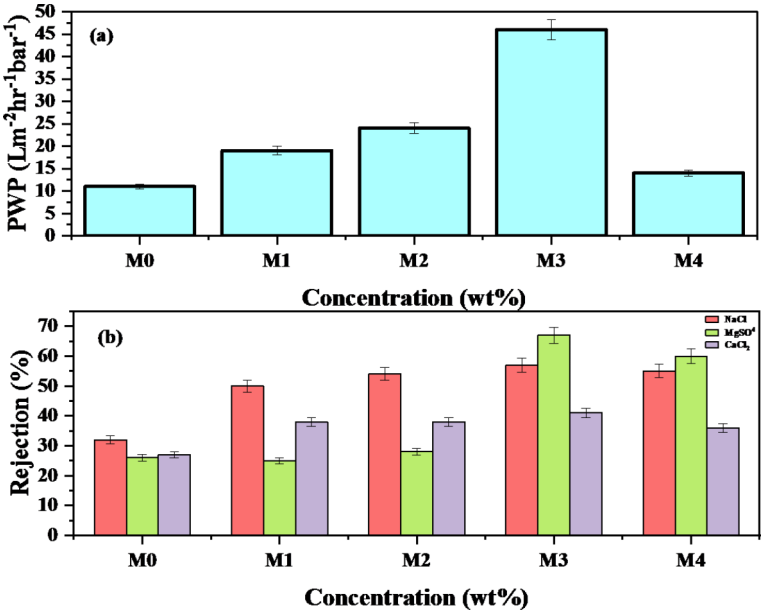


**Fig. 7**. Membrane performance, (**a**) effect of AgNPs loading on pure water permeability, (**b**) effect of AgNPs loading on salts rejection.

flow resistance. However, at 1 wt% AgNPs concentration, the PWP decreased slightly, although it remained higher the neat membrane. This reduction could be due to reaching a the limiting mass percentage[53]. The higher nanoparticles loading often leads to aggregation and/or increased viscosity of the casting solution, resulting into a denser structure with fewer macro-voids and interconnected pores thus reducing water permeability[52].

The salt rejection performance of the MMMs was tested using three salts: sodium chloride (NaCl), magnesium sulfate ($MgSO_4$), and calcium chloride ($CaCl_2$), and the results are shown in Fig. 7b. The addition of AgNPs improved salt rejection for all tested salts. At 0.75 wt% AgNPs loading, NaCl rejection increased from 32 to 57%, $MgSO_4$ from 26 to 67%, and $CaCl_2$ from 27 to 41%. The higher rejection of NaCl (a monovalent salt) compared to divalent salts ($MgSO_4$ and $CaCl_2$) till 0.5wt.% AgNPs was likely due to its dissociation into $Na^+$ and $Cl^-$ ions, which experience less electrostatic repulsion than divalent ions. But at optimal concentration of AgNPs which was 0.75wt.% the membrane show more rejection of $MgSO_4$ (Bivalent ion) and even at 1wt.% as compared to NaCl. As reported in earlier reported study[54], the bivalent ions shows less ion transmission as compared to monovalent. Additionally, the negative surface charge of NF membranes effectively repels $Cl^-$ ions, resulting in higher rejection rates. Moreover the osmotic effects and ions interaction with membrane also leads to higher rejection of NaCl[55].

The lower rejection of $CaCl_2$ could be attributed to the positive charge of calcium ions, which are attracted to the membrane surface due to Donnan exclusion. This principle suggests that ions with higher negative charges are more likely to be blocked, while positively charged ions may pass more easily[56]. In PES/AgNPs membranes, the positive calcium ions ($Ca^{2+}$) from calcium chloride ($CaCl_2$) are attracted to the negatively charged membrane surface, which in turn affects the zeta potential by decreasing the overall surface charge. This reduction in zeta potential weakens the membrane's natural ability to repel $Ca^{2+}$ ions, allowing these ions to pass through more easily, especially at higher salt concentrations where the membrane's electric field is less effective[57].

AgNPs also add unique surface properties that may encourage selective ion adsorption. AgNPs can modify how ions interact with the membrane, affecting both Donnan exclusion and ion binding. Moreover, as feed concentration was 1000ppm, the higher $Cl^-$ concentrations can promote the formation of uncharged and negatively charged complexes with metal ions like $Ca^{2+}$. For $CaCl_2$, as $Cl^-$ concentration rises, uncharged or negatively charged $CaCl_3^-$ and $CaCl_4^{2-}$ complexes may form. This shift reduces the interaction between $Ca^{2+}$ ions and the negatively charged PES/AgNPs membrane, as fewer free $Ca^{2+}$ ions are available to be repelled by the membrane surface[58].

In case of $MgSO_4$, the initial rejection was low but significantly improved at 0.75 wt% AgNPs, likely due to enhanced Donnan exclusion and the catalytic properties of AgNPs. The increase in nanofillers reduces the dielectric constant of the polymer matrix, improving the exclusion of negatively charged ions. This may be due to the improved morphology of PES/AgNPs with uniform distribution of pores and maintaining a sufficiently dense layer as shown in SEM images. Further increases in AgNPs to 1 wt% resulted in a slight decline in rejection, which could be attributed by SEM images that, the thinning of the dense top layer or nanoparticle aggregation, creating non-uniform pore structures that allow salts to pass through more easily. Moreover, when the concentration of nanofillers exceeds the optimal mass percentage, nanoparticles aggregate, forming dense clusters that disrupt the uniform pore structure. This results in non-selective or irregular pores, allowing salt ions to pass through more easily and lowering salt rejection[52].

Industrial wastewater originating from textiles contains hazardous dyes that necessitate effective removal. The incorporation of AgNPs into PES membranes enhances not only salt rejection and water permeability but also dye rejection, thanks to the catalytic, hydrophilic, and surface-charge-modifying properties of AgNPs. Three model dyes were used for this evaluation: Methylene Blue (MB, Mw = 373 g/mol), Congo Red (CR, Mw = 696 g/mol), and Rose Bengal (RB, Mw = 1017 g/mol). The rejection of smaller molecules like Methylene Blue was particularly effective with AgNPs-loaded membranes, demonstrating superior performance. Figure 8 illustrates the rejection efficiency for Methylene Blue using both controlled PES and PES/AgNPs membranes at a 30 ppm dye concentration.

Zeta potential measurements revealed that PES/AgNPs membranes at 0.75 wt% exhibited more positive surface charges at pH 3 and 5, and less negative charges at pH 7, compared to neat membranes, which remained negatively charged at neutral pH. For Methylene Blue, a cationic dye, the stronger negative charge of the neat PES membrane likely caused more adsorption of the dye, leading to lower rejection and higher fouling. In contrast, the 0.75 wt% AgNPs membrane exhibited less negative zeta potential at neutral pH, resulting in less adsorption and higher rejection efficiency. Additionally, the higher repulsive forces at lower pH levels enhanced dye rejection. The hydrophilicity and pore architecture of the AgNP-modified membranes also played a role in improving Methylene Blue rejection.

Congo Red, an anionic dye, demonstrated enhanced rejection with the incorporation of AgNPs, likely due to the strong electrostatic repulsion between the negatively charged dye and the membrane surface, leading to nearly 100% rejection. Size exclusion may have also contributed, as Congo Red is a large molecule and may accumulate on the membrane surface, thus being blocked by the pores[58]. In contrast, Rose Bengal, despite having a slightly smaller molecular size than Congo Red, exhibited lower rejection. Rose Bengal's strong negative charge and the membrane's charge characteristics at different pH levels influenced its rejection. AgNPs within the membrane matrix thus provides additional surface charges and adsorption sites, facilitating the binding of dye molecules through electrostatic interactions and physical adsorption.

Membrane fouling is an inevitable challenge in nanofiltration, particularly in industrial applications. Understanding the relationship between membrane structure, physicochemical properties, and resistance to fouling is crucial for optimizing membrane performance. In this study, Sodium Alginate (SA, Mw = 216.121 g/mol) was used as a foulant to evaluate antifouling performance. The addition of AgNPs significantly enhanced membrane properties, including antimicrobial action, improved hydrophilicity, reduced protein adsorption, and

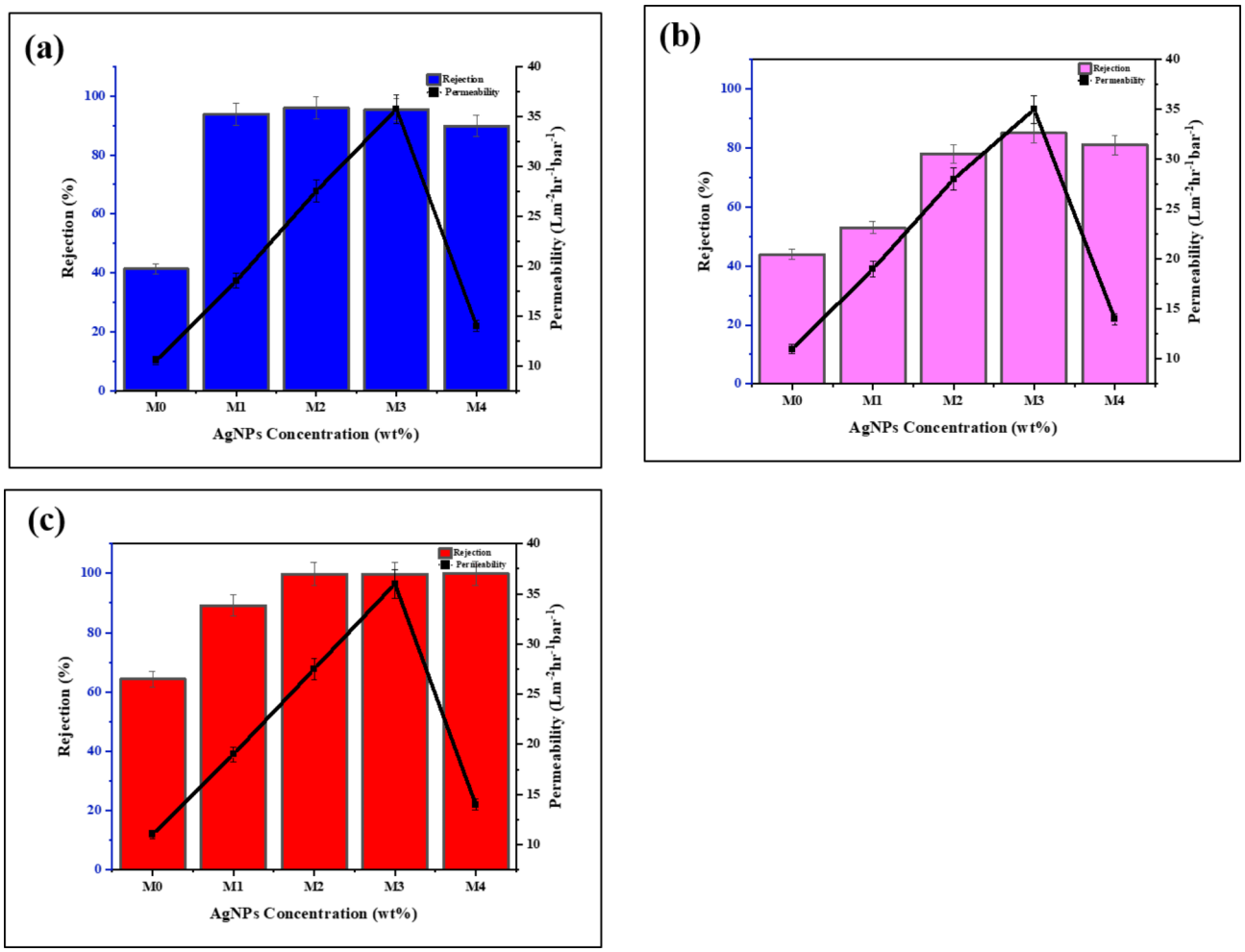


**Fig. 8**. Dye rejection performance of membranes: rejection percentages for (**a**) Methylene Blue, (**b**) Rose Bengal, and (**c**) Congo Red.

modified surface charge.These enhancements contributed to the superior antifouling capacity of the PES/AgNP membranes compared to the neat PES membrane.

As shown in Fig. 9a, the membrane with 0.75 wt% AgNPs exhibited the best antifouling performance. The flux decline for the neat PES membrane was more rapid, with limited flux recovery after backwashing, indicating higher fouling susceptibility. In contrast, the 0.75 wt% AgNPs membrane maintained higher flux throughout the test, with better recovery after fouling. At 1 wt% AgNPs, a slight reduction in filtration efficiency was observed. This could be attributed to nanoparticle aggregation and increased surface roughness, favoring fouling formation. Excessive nanoparticle loading may cause pore blockage and uneven membrane morphology, highlighting the importance of controlling AgNP concentration to minimize fouling and optimize performance.

The flux recovery ratio (FRR) was highest for the 0.75 wt% AgNPs membrane, achieving 98.7% recovery, compared to 69.09% for the neat PES membrane and 90.6% for the 1 wt% AgNPs membrane. Similarly, the fouling resistance ratios showed distinct differences between the membranes. The neat PES membrane exhibited 36% reversible fouling (RF), 30% irreversible fouling (IRF), and a total fouling (TF) of 67%. In contrast, the 0.75 wt% AgNPs membrane showed superior results with 55% RF, only 1.2% IRF, and 56% TF, indicating minimal irreversible fouling. The 1 wt% AgNPs membrane, while slightly outperforming the neat membrane, exhibited higher irreversible fouling (9.3%) due to nanoparticle aggregation.

The membrane surface charge plays a crucial role in resisting fouling. Membranes with more negative charges are more likely to repel negatively charged foulants, such as sodium alginate, which helps reduce fouling. However, the results also show that the addition of AgNPs significantly improves antifouling properties, even in membranes with less negative zeta potential (e.g., M3). The hydrophilic nature of AgNPs can promote the formation of a thin hydration layer on the membrane surface, creating a barrier that limits direct contact between the membrane and sodium alginate. This hydration layer acts as a physical and chemical shield, minimizing alginate adhesion and enhancing fouling resistance. These findings suggest that both surface charge and AgNP properties work together to enhance fouling resistance. The 0.75 wt% AgNPs membrane demonstrates the best performance, with a high level of reversible fouling and minimal irreversible fouling, indicating that it achieves an optimal balance between surface charge and AgNP effects. The antibacterial properties of AgNPs also

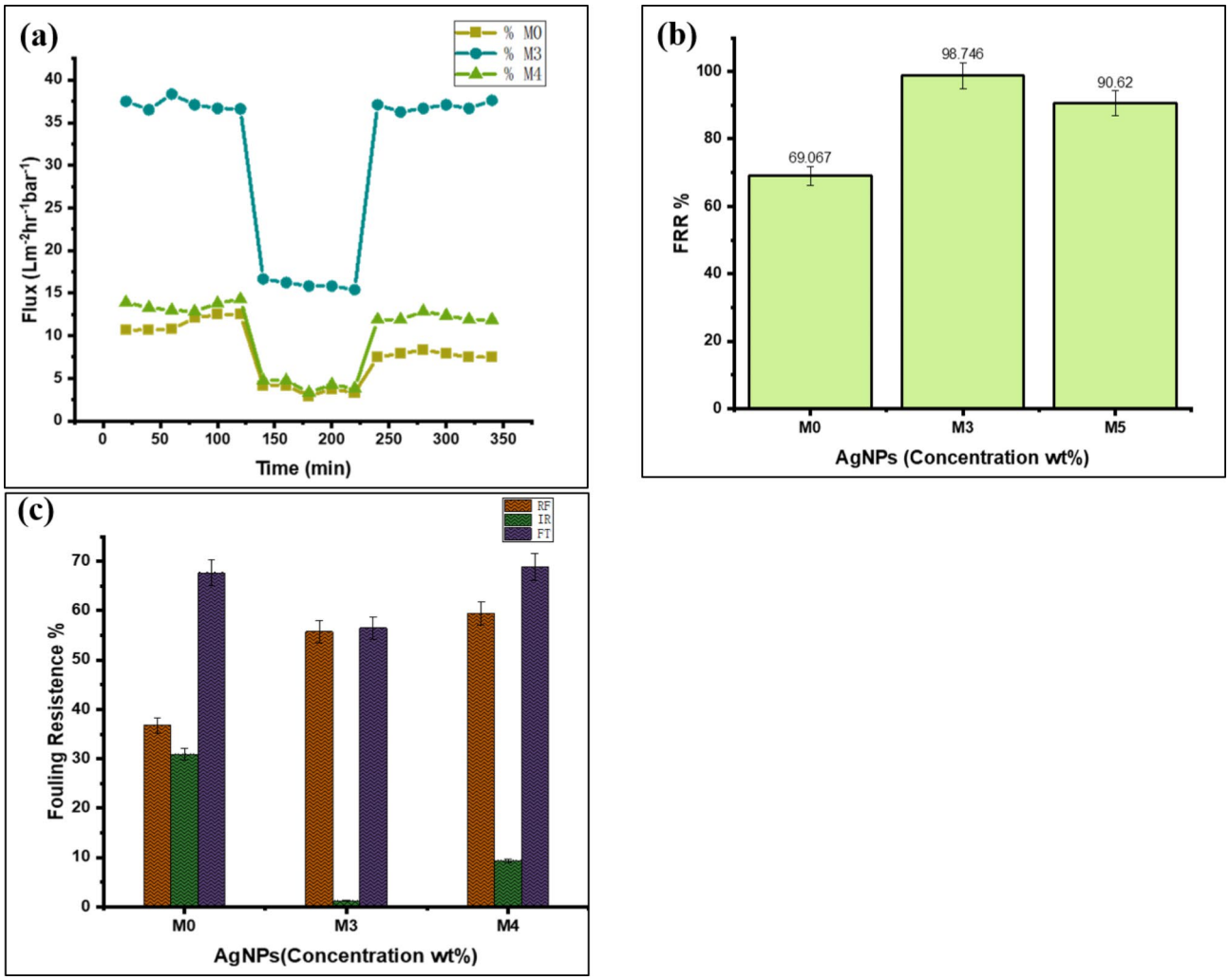


**Fig. 9**. Antifouling capacity of the prepared MMMs (**a**), Flux recover ratio (**b**), Fouling Resistance ration (**c**).

contributed to reducing biofouling, as previously reported[59]. These results highlight the importance of optimal nanoparticle concentration. The effective incorporation of AgNPs thus improved membrane surface properties, reduced fouling, and minimized the deposition of contaminants.

## Conclusions

This study successfully demonstrated the fabrication and characterization of MMMs incorporating green-synthesized AgNPs using *Hibiscus Rosa sinensis* extract. The integration of AgNPs into the PES matrix led to significant improvements in membrane performance, particularly in terms of pure water permeability, salt rejection, dye removal, and antifouling properties, positioning these membranes into nanofiltration range. The membrane with 0.75 wt% AgNPs exhibited the best overall performance, showing the highest pure water permeability and optimal rejection rates for NaCl, $MgSO_4$, and $CaCl_2$ suitable for loose nanofiltration application. This enhancement was primarily attributed to increased porosity, larger pore size, and improved hydrophilicity due to the presence of AgNPs. In terms of dye rejection, the AgNP-modified membranes demonstrated superior capabilities, particularly for Methylene Blue and Congo Red, with rejection rates reaching up to 100% at higher AgNP concentrations. The antifouling tests revealed that the 0.75 wt% AgNPs membrane exhibited minimal irreversible fouling and high flux recovery, making it the most effective in resisting fouling. Overall, this study highlights the potential of green-synthesized AgNPs as effective nanofillers for enhancing the performance of MMMs for nanofiltration application. Several areas require further investigation to optimize membrane performance, particularly in enhancing the rejection of Rose Bengal and similar organic pollutants. Additionally, scaling up the green synthesis of AgNPs should be considered to assess the feasibility of larger-scale production for industrial applications, ensuring consistent membrane performance in real-world scenarios.

## Declaration of generative AI

During the preparation of this work, the authors used ChatGPT to refine writing and improve readability. The authors have reviewed and edited the AI-generated content as necessary and take full responsibility for the contents of this publication.

## Data availability

All data generated or analysed during this study are included in this published article.

Received: 27 September 2024; Accepted: 17 December 2024
Published online: 06 January 2025

## References

1. He, C. et al. Future global urban water scarcity and potential solutions. *Nat. Commun.* **12** (1), 4667 (2021).
2. Singh, N. et al. Challenges of water contamination in urban areas, in Current Directions in Water Scarcity Research, vol. 6, 173–202 (Elsevier, 2022).
3. Ismail, M. et al. Pollution, toxicity and carcinogenicity of organic dyes and their catalytic bio-remediation. *Curr. Pharm. Des.* **25** (34), 3645–3663 (2019).
4. Akinnawo, S. O., Ayadi, P. O. & Oluwalope, M. T. Chemical coagulation and biological techniques for wastewater treatment. *Ovidius Univ. Ann. Chem.* **34** (1), 14–21 (2023).
5. Sukmana, H., Bellahsen, N., Pantoja, F. & Hodur, C. Adsorption and coagulation in wastewater treatment–review. *Prog Agric. Eng. Sci.* **17** (1), 49–68 (2021).
6. Goh, P. S., Lau, W. J., Othman, M. H. D. & Ismail, A. F. Membrane fouling in desalination and its mitigation strategies. *Desalination* **425**, 130–155 (2018).
7. Maalige, R. N. et al. Low operating pressure nanofiltration membrane with functionalized natural nanoclay as antifouling and flux promoting agent. *Chem. Eng. J.* **358**, 821–830 (2019).
8. Feng, X., Peng, D., Zhu, J., Wang, Y. & Zhang, Y. Recent advances of loose nanofiltration membranes for dye/salt separation. *Sep. Purif. Technol.* **285**, 120228 (2022).
9. Dong, Y., Wu, H., Yang, F. & Gray, S. Cost and efficiency perspectives of ceramic membranes for water treatment. *Water Res.* **220**, 118629 (2022).
10. Khan, S. & Iqbal, A. Organic polymers revolution: applications and formation strategies, and future perspectives. *J. Polym. Sci. Eng.* **6** (1), 3125 (2023).
11. Karami, P. et al. Thermally stable thin film composite polymeric membranes for water treatment: a review. *J. Clean. Prod.* **250**, 119447 (2020).
12. Shukla, A. K., Alam, J. & Alhoshan, M. Recent advancements in polyphenylsulfone membrane modification methods for separation applications. *Membr. (Basel).* **12** (2), 247 (2022).
13. Otitoju, T. A., Ahmad, A. L. & Ooi, B. S. Recent advances in hydrophilic modification and performance of polyethersulfone (PES) membrane via additive blending. *RSC Adv.* **8** (40), 22710–22728 (2018).
14. Goh, P. S., Wong, K. C. & Ismail, A. F. Membrane technology: a versatile tool for saline wastewater treatment and resource recovery. *Desalination* **521**, 115377 (2022).
15. Elrasheedy, A., Nady, N., Bassyouni, M. & El-Shazly, A. Metal organic framework based Polymer mixed matrix membranes: review on applications in water purification. *Membr. (Basel).* **9** (7), 88 (2019).
16. Baghbanzadeh, M., Rana, D., Lan, C. Q. & Matsuura, T. Effects of inorganic nano-additives on properties and performance of polymeric membranes in water treatment. *Sep. Purif. Rev.* **45** (2), 141–167 (2016).
17. Alkhouzaam, A. & Khraisheh, M. Development of eco-friendly coating for the fabrication of high performing loose nanofiltration membranes for dye-contaminated wastewater treatment. *Desalination* **581**, 117609 (2024).
18. Chong, W. C., Koo, C. H. & Lau, W. J. Mixed-matrix membranes incorporated with functionalized nanomaterials for water applications. *Handb. Funct. Nanomater Ind. Appl.*, pp. 15–51 (2020).
19. Al-Maliki, R. M., Al-Naqbi, A. H. & Alshammari, M. M. Classification of nanomaterials and the effect of graphene oxide (GO) and recently developed nanoparticles on the ultrafiltration membrane and their applications: a review. *Membr. (Basel).* **12** (11), 1043. https://doi.org/10.3390/membranes12111043 (2022).
20. Rasool, A., Sri, S., Zulfajri, M. & Krismastuti, F. S. H. Nature inspired nanomaterials, advancements in green synthesis for biological sustainability. *Inorg. Chem. Commun.*, 112954, (2024).
21. Kumar, J. A., Suman, M., Sharma, P. & Gupta, R. A focus on the green synthesis of metal/metal-based oxide nanoparticles: Various mechanisms and applications towards an ecological approach. *Journal of Cleaner Production, 324*, 129198. https://doi.org/10.1016/j.jclepro.2021.129198J (2021).
22. Ahmed, S. F. et al. Green approaches in synthesising nanomaterials for environmental nanobioremediation: Technological advancements, applications, benefits and challenges. *Environ. Res.* **204**, 111967 (2022).
23. Timoszyk, A. & Grochowalska, R. Mechanism and antibacterial activity of gold nanoparticles (AuNPs) functionalized with natural compounds from plants. *Pharmaceutics* **14** (12), 2599 (2022).
24. Salih, A. M. et al. Biogenic silver nanoparticles improve bioactive compounds in medicinal plant Juniperus procera in vitro. *Front. Plant. Sci.* **13**, 962112 (2022).
25. Restrepo, C. V. & Villa, C. C. Synthesis of silver nanoparticles, influence of capping agents, and dependence on size and shape: a review. *Environ. Nanatechnol. Monit. Manag.* **15**, 100428 (2021).
26. Lu, Y., Jia, J., Miao, H., Ruan, W. & Wang, X. Performance improvement and biofouling mitigation in osmotic microbial fuel cells via in situ formation of silver nanoparticles on forward osmosis membrane. *Membr. (Basel).* **10** (6), 122 (2020).
27. Alnairat, N. et al. Green synthesis of silver nanoparticles as an effective antibiofouling material for polyvinylidene fluoride (PVDF) ultrafiltration membrane. *Polym. (Basel).* **13** (21), 3683 (2021).
28. Azhar, F. H. et al. A study of different concentrations of bio-silver nanoparticles in polysulfone mixed matrix membranes in water separation performance. *J. Water Process. Eng.* **38**, 101575 (2020).
29. Gonca, S., Arslan, H., Isik, Z., Özdemir, S. & Dizge, N. The surface modification of ultrafiltration membrane with silver nanoparticles using Verbascum thapsus leaf extract using green synthesis phenomena. *Surf. Interfaces.* **26**, 101291 (2021).
30. Rao, B. L., Gouda, G. P. & Shivananda, C. S. Green synthesis of silver nanoparticles using Hibiscus Rosa Sinensis flower extract, in AIP Conference Proceedings, AIP Publishing, (2020).
31. Nayak, D., Ashe, S., Rauta, P. R. & Nayak, B. Biosynthesis, characterisation and antimicrobial activity of silver nanoparticles using Hibiscus rosa-sinensis petals extracts. *IET Nanobiotechnol.* **9** (5), 288–293 (2015).
32. Rani, P. et al. Highly stable AgNPs prepared via a novel green approach for catalytic and photocatalytic removal of biological and non-biological pollutants. *Environ. Int.* **143**, 105924. https://doi.org/10.1016/j.envint.2020.105924 (2020).
33. David, L. & Moldovan, B. Green synthesis of biogenic silver nanoparticles for efficient catalytic removal of harmful organic dyes. *Nanomaterials* **10** (2), 202 (2020).

34. Surya, S., Kumar, G. D. & Rajakumar, R. Green synthesis of silver nanoparticles from flower extract of Hibiscus rosa-sinensis and its antibacterial activity. *Int. J. Innov. Res. Sci. Eng. Technol.* **5** (4), 5242–5247 (2016).
35. Alharbi, N. S., Alsubhi, N. S. & Felimban, A. I. Green synthesis of silver nanoparticles using medicinal plants: characterization and application. *J. Radiat. Res. Appl. Sci.* **15** (3), 109–124. https://doi.org/10.1016/j.jrras.2022.06.012 (2022).
36. Bykkam, S., Ahmadipour, M., Narisngam, S., Kalagadda, V. R. & Chidurala, S. C. Extensive studies on X-ray diffraction of green synthesized silver nanoparticles. *Adv. Nanopart.* **4** (1), 1–10 (2015).
37. Mehta, B. K., Chhajlani, M. & Shrivastava, B. D. Green synthesis of silver nanoparticles and their characterization by XRD, in Journal of physics: conference series, IOP Publishing, p. 12050. (2017).
38. Parthiban, E., Manivannan, N., Ramanibai, R. & Mathivanan, N. Green synthesis of silver-nanoparticles from Annona reticulata leaves aqueous extract and its mosquito larvicidal and anti-microbial activity on human pathogens. *Biotechnol. Rep.* **21**, e00297 (2019).
39. Dhaka, A. et al. A review on biological synthesis of silver nanoparticles and their potential applications. *Results Chem.* **101**, 108 (2023).
40. Karahan, H. A. & Colgecen, H. Silver nanoparticles production mediated by natural tetraploid Trifolium pratense L.: characterization and potential biological activity. *Acta Agrobot*, **76**, (2023).
41. Santhosh, S. B., Ragavendran, C. & Natarajan, D. Spectral and HRTEM analyses of Annona muricata leaf extract mediated silver nanoparticles and its larvicidal efficacy against three mosquito vectors Anopheles Stephensi, Culex quinquefasciatus, and Aedes aegypti. *J. Photochem. Photobiol B Biol.* **153**, 184–190 (2015).
42. Narayanan, M. et al. Green synthesis of silver nanoparticles from aqueous extract of Ctenolepis Garcini L. and assess their possible biological applications. *Process. Biochem.* **107**, 91–99 (2021).
43. Kambale, E. K. et al. Green synthesis of antimicrobial silver nanoparticles using aqueous leaf extracts from three Congolese plant species (Brillantaisia Patula, Crossopteryx febrifuga and Senna siamea). *Heliyon* **6**, 8 (2020).
44. Šupová, M., Martynková, G. S. & Barabaszová, K. Effect of nanofillers dispersion in polymer matrices: a review. *Sci. Adv. Mater.* **3** (1), 1–25 (2011).
45. Ying, S. et al. Green synthesis of nanoparticles: current developments and limitations. *Environ. Technol. Innov.* **26**, 102336 (2022).
46. Ahmad, T. & Guria, C. Progress in the modification of polyvinyl chloride (PVC) membranes: a performance review for wastewater treatment. *J. Water Process. Eng.* **45**, 102466 (2022).
47. Haider, M. S. et al. Aminated polyethersulfone-silver nanoparticles (AgNPs-APES) composite membranes with controlled silver ion release for antibacterial and water treatment applications. *Mater. Sci. Eng. C.* **62**, 732–745 (2016).
48. Mihaylov, M. Y. et al. FTIR and density functional study of NO interaction with reduced ceria: identification of N3 – and NO2 – as new intermediates in NO conversion. *Appl. Catal. B.* **176**, 107–119 (2015).
49. Andrade, P. F., de Faria, A. F., Oliveira, S. R., Arruda, M. A. Z. & Carmo Gonçalves, M. do Improved antibacterial activity of nanofiltration polysulfone membranes modified with silver nanoparticles. Water Research, 81, 333–342. (2015). https://doi.org/10.1016/j.watres.2015.05.010
50. Al Mahrouqi, D., Vinogradov, J. & Jackson, M. D. Zeta potential of artificial and natural calcite in aqueous solution. *Adv. Colloid Interface Sci.* **240**, 60–76 (2017).
51. Burns, D. B. & Zydney, A. L. Buffer effects on the Zeta potential of ultrafiltration membranes. *J. Memb. Sci.* **172** (1–2), 39–48 (2000).
52. Taha, Y. R. et al. Optimum content of incorporated nanomaterials: characterizations and performance of mixed matrix membranes a review. *Desalin. Water Treat.*, p. 100088, (2024).
53. Alkhouzaam, A. & Qiblawey, H. Functional GO-based membranes for water treatment and desalination: fabrication methods, performance and advantages. A review. *Chemosphere* **274**, 129853 (2021).
54. Ramadan, Y., Pátzay, G. & Szabó, G. T. Transport of NaCl, $MgSO_4$, $MgCl_2$ and $Na_2SO_4$ across DL type nanofiltration membrane. *Period Polytech. Chem. Eng.* **54** (2), 81–86 (2010).
55. Acar, S., Cengİz, H. Y., ErgÜn, A., Konyali, E. & DelİgÖz, H. A comparative study on the monovalent and divalent cation separation of polymeric films and membranes from salt solutions under diffusion-dialysis. *Turkish J. Chem.* **44** (4), 1134–1147 (2020).
56. Suhalim, N. S. et al. Rejection mechanism of ionic solute removal by nanofiltration membranes: an overview. 12(**3**), 437 (2022).
57. Salgın, S., Salgın, U. & Soyer, N. Streaming potential measurements of polyethersulfone ultrafiltration membranes to determine salt effects on membrane zeta potential. *Int. J. Electrochem. Sci.*, **8**(3), 4073–4084 (2011).
58. Choudhury, R. R., Gohil, J. M., Mohanty, S. & Nayak, S. K. Antifouling, fouling release, and antimicrobial materials for surface modification of reverse osmosis and nanofiltration membranes. *J. Mater. Chem. A.* **6** (2), 313–333. https://doi.org/10.1039/C7TA09137A (2018).
59. Yin, J., Yang, Y., Hu, Z. & Deng, B. Attachment of silver nanoparticles (AgNPs) onto thin-film composite (TFC) membranes through covalent bonding to reduce membrane biofouling. *J. Memb. Sci.* **441**, 73–82 (2013).


## Acknowledgements

Nusrat Bashir (Ph.D scholar) and Dr.Muhammad Afzaal(Supervisor) are thankful the Office of Research Innovation & Commercialization Government College University (GCU), Lahore, Pakistan, for Ph.D. research funding and ORIC research project(NO/98/ORIC/23) to complete this research work. The authors also extend the appreciation to the Researchers Supporting Project number (RSPD2025R189) King Saud University, Riyadh, Saud Arabia.

## Author contributions

Conceptualization, original draft writing, reviewing, and editing: Nusrat Bashir, Muhammad Afzaal, Asim Laeeq Khan. Formal analysis, investigations, funding acquisition, reviewing, and editing: Rab Nawaz, Ali Irfan, Khalid S. Almaary. Resources, data validation, data curation, and supervision: Fakhreldeen Dabiellil, Mohammed Bourhia, Zulkifl Ahmed.

## Declarations

## Competing interests

The authors declare no competing interests.

## Additional information

**Supplementary Information** The online version contains supplementary material available at https://doi.org/10.1038/s41598-024-83801-w.

**Correspondence** and requests for materials should be addressed to M.A., A.I. or F.D.

**Reprints and permissions information** is available at www.nature.com/reprints.

**Publisher's note** Springer Nature remains neutral with regard to jurisdictional claims in published maps and institutional affiliations.

**Open Access** This article is licensed under a Creative Commons Attribution-NonCommercial-NoDerivatives 4.0 International License, which permits any non-commercial use, sharing, distribution and reproduction in any medium or format, as long as you give appropriate credit to the original author(s) and the source, provide a link to the Creative Commons licence, and indicate if you modified the licensed material. You do not have permission under this licence to share adapted material derived from this article or parts of it. The images or other third party material in this article are included in the article's Creative Commons licence, unless indicated otherwise in a credit line to the material. If material is not included in the article's Creative Commons licence and your intended use is not permitted by statutory regulation or exceeds the permitted use, you will need to obtain permission directly from the copyright holder. To view a copy of this licence, visit http://creativecommons.org/licenses/by-nc-nd/4.0/.

© The Author(s) 2025